

Coherent microwave scattering from xenon resonance-enhanced multiphoton ionization-initiated plasma in air

Cite as: J. Appl. Phys. **127**, 053301 (2020); <https://doi.org/10.1063/1.5135316>

Submitted: 05 November 2019 . Accepted: 22 January 2020 . Published Online: 04 February 2020

Christopher A. Galea , Mikhail N. Shneider , Mark Gragston , and Zhili Zhang 



View Online



Export Citation



CrossMark

Lock-in Amplifiers
Find out more today



 Zurich
Instruments



Coherent microwave scattering from xenon resonance-enhanced multiphoton ionization-initiated plasma in air

Cite as: J. Appl. Phys. 127, 053301 (2020); doi: 10.1063/1.5135316

Submitted: 5 November 2019 · Accepted: 22 January 2020 ·

Published Online: 4 February 2020



View Online



Export Citation



CrossMark

Christopher A. Galea,^{1,a)} Mikhail N. Shneider,¹ Mark Cragston,² and Zhili Zhang²

AFFILIATIONS

¹Department of Mechanical and Aerospace Engineering, Princeton University, Princeton, New Jersey 08544, USA

²Department of Mechanical, Aerospace, and Biomedical Engineering, University of Tennessee, Knoxville, Tennessee 37996, USA

^{a)}Author to whom correspondence should be addressed: cgalea@princeton.edu

ABSTRACT

Here we present the experimental and computational study of resonance-enhanced multiphoton ionization (REMPI) of xenon and subsequent avalanche ionization of air. Xenon was excited from the ground state to the excited 6p state ($89\,162\text{ cm}^{-1}$) by two photons at 224.3 nm. The third photon at 224.3 nm subsequently produced ionization of xenon in air. The seed electrons from the ionization served as the medium to further absorb the laser pulse for the rotational and vibrational excitation and avalanche ionization of O_2 and N_2 . Plasma chemistry of O_2 and N_2 in air was included in the model. The results are useful for understanding REMPI-initiated plasma in air and possibly new diagnostics tools based on REMPI-initiated plasma emissions.

Published under license by AIP Publishing. <https://doi.org/10.1063/1.5135316>

I. INTRODUCTION

Detection and analysis of trace gas species remains important for air quality control, nuclear proliferation monitoring, and combustion characterization. A variety of laser diagnostic techniques have been used for such measurements, including tunable diode laser absorption spectroscopy (TDLAS), Laser-Induced Breakdown Spectroscopy (LIBS), and laser-induced fluorescence (LIF). Though simple to set up, TDLAS cannot provide spatially resolved measurements, and LIBS measurements are typically not able to provide quantitative information. LIF techniques can provide quantitative and spatially resolved information, but fluorescent signal intensities generally require intensified cameras or temporal averaging, and more importantly, the quenching of fluorescence signals requires the careful calibration of components. Radar resonance-enhanced multiphoton ionization (REMPI) is a technique that uses coherent microwave scattering on a small plasma created from selective multiphoton ionization of the target species. The coherent microwave Rayleigh scattering effectively counts the free electrons in the resulting weak plasma, which also provides a measurement of species concentration.^{1,2} Furthermore, since multiphoton processes require high-intensity laser radiation,

the measurement volume is spatially limited to the focal volume, which provides high-spatial resolution. Radar REMPI has been used for a variety of quantitative measurements, including flame temperature,³ atomic oxygen concentration in plasmas,⁴ radical species generation,⁵ and the detection of trace gases.⁶ It has also been shown to be effective for measurements in scenarios with limited optical access, given that ceramic materials are generally microwave transparent.^{7,8}

In order to properly extract quantitative data from Radar REMPI measurements, it is important to understand the dynamics associated with REMPI plasma. Dynamics of interest include ionization and recombination rates, avalanche ionization effects, and the effects of nontargeted species on the plasma development. In this work, a model is developed and compared to experimental measurements to understand the dynamics of a REMPI plasma generated in a low pressure mixture of xenon and air.

Xenon has an abundance of well-known spectroscopic properties and multiphoton absorption cross sections and is often used as a calibration gas for two-photon laser-induced fluorescence.⁹ Furthermore, xenon is a trace gas in the atmosphere that can be monitored for nonproliferation applications.¹⁰ Trace xenon has been detected down to 1 ppm in an atmospheric helium buffer

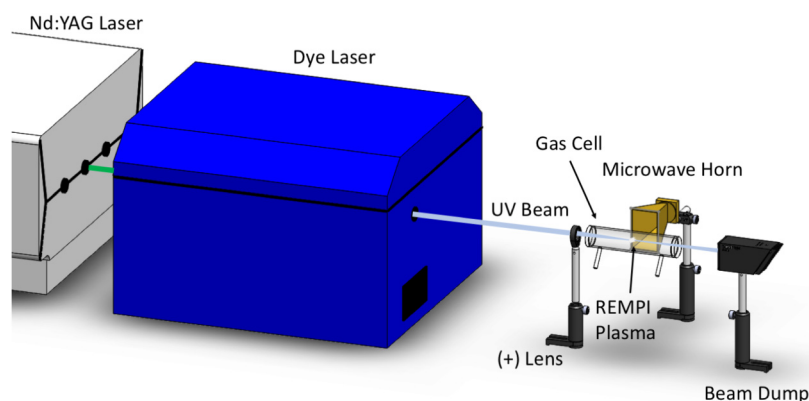


FIG. 1. The experimental setup used for coherent Rayleigh microwave scattering measurements of xenon REMPI-initiated plasma in a 174 Torr xenon–air mixture.

gas.¹¹ Given the signal-to-noise ratio of the 1 ppm xenon signal, trace xenon may potentially be detectable down to 100 ppb. In this paper, xenon was probed by REMPI in air. The temporal evolution of the REMPI-initiated plasma was tracked by the coherent microwave scattering and modeled by plasma kinetics. Section II provides details regarding the experimental measurements, and Sec. III shows the experimental results. Section IV discusses the formulation of a 0-dimensional kinetic model to compare with the experimental results, while Sec. V discusses the comparisons. Finally, the results are summarized in Sec. VI.

II. EXPERIMENTAL SETUP

Figure 1 shows the experimental setup used for xenon Radar REMPI measurements. A 10 Hz Nd:YAG laser (Spectra Pro 230) was used to pump a dye laser (Sirah PrecisionScan, Rodmine 6G as the dye) to produce 568.4 nm. The mixing of residual 1064 nm

from the Nd:YAG laser and frequency doubled 568.4 nm was achieved to output at 224.3 nm. The linewidth of 1064 nm is about $1\text{--}2\text{ cm}^{-1}$, which leads to the linewidth of 0.02 nm for the mixing output at 224 nm. The output laser energy at 224.3 nm can be up to 10 mJ/pulse. The spectral scanning can be achieved by moving the gratings inside the dye laser. A continuous scanning around 224.3 nm might induce slight fluctuations of about 0.2 mJ/pulse due to slight variation of the mixing crystal. The fluctuations have been recorded by a power meter, which were used to normalize the final REMPI spectra. The 224.3 nm beam was focused using a 100 mm fused silica plano-convex lens to achieve the high intensity needed for REMPI of xenon. The ground and the excited states of xenon are $5p^6$ and $5p^56p$ ($89\,162\text{ cm}^{-1}$), respectively.

The coherent microwave scattering system used for this work is identical to that described in previous works and is shown in Fig. 2.^{4,5} Briefly, a 10-dBm tunable microwave source (HP 8350B

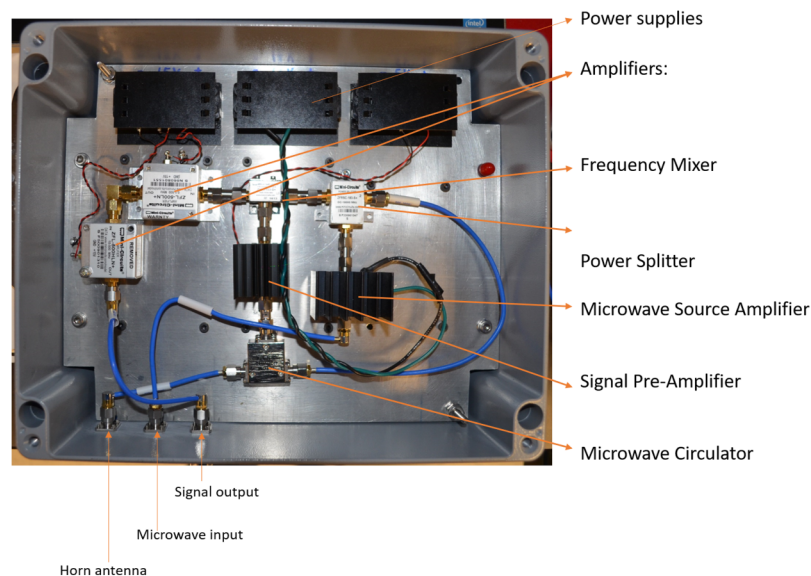


FIG. 2. Microwave setup used for coherent Rayleigh microwave scattering measurements of xenon REMPI-initiated plasma in a 174 Torr xenon–air mixture. The whole box is 11 in. (L) \times 9 in. (W) \times 4.5 in. (H).

sweep oscillator, set at ~ 10 GHz) was applied in the homodyne transceiver detection system (MDS). The microwave source was first split into two channels. One of them was used to illuminate the ionization point through a microwave horn (WR75, 15-dB gain). Microwave scattering from the plasma was collected by the same microwave horn. The received microwave passed through a microwave circulator and was amplified 30 dB by one preamplifier at ~ 10 GHz. After the frequency was converted down in the mixer, two other amplifiers with a bandwidth of 2.5 kHz–1.0 GHz amplified the signal by another factor of 60 dB. From the geometry of dipole radiation, the polarization of the microwave was chosen to be along the propagation direction of the laser beam to maximize the scattering signal. Xenon and air were mixed by partial pressure to 174 Torr inside the gas cell, with 0.6% Xe and 99.4% air.

III. MICROWAVE SCATTERING MEASUREMENTS

Confirmation of $2 + 1$ REMPI of xenon was determined by spectral scanning of the dye laser and monitoring the amplitude of the microwave scattering signal. Figure 3(a) shows that peak excitation of xenon occurs at 224.3 nm for a xenon–nitrogen gas mixture at 760 Torr, which confirms successful selective ionization of xenon. Figure 3(b) shows signal waveforms for microwave scattering on the REMPI plasma produced in a 174 Torr xenon–air mixture. It should be noted that due to the strong resonance of REMPI xenon, the xenon emissions can become visible. At low laser excitation energy, TALIF (Two-photon Absorption Laser-Induced Fluorescence) was generally identified at 834.68 nm. At high laser excitation energy, a bright white emission line near the laser focus can be identified for up to a length of 1 cm, which is the evidence of REMPI-initiated plasma emissions.

IV. MODEL FORMULATION

We present here a 0-dimensional kinetic model for the 1 Torr xenon, 173 Torr air mixture. The model includes electrons, xenon

atoms, ions, two-photon excited state atoms, and dimer ions; diatomic oxygen molecules and positive and negative ions; and diatomic nitrogen molecules. In the 0-dimensional model, the Radar REMPI signal (which is directly proportional to the scattered electric field as a result of homodyne mixing) has the following functional form in the Rayleigh regime ($L_p \ll \lambda_{MW} \ll R$ and $L_p < \delta_d$, where L_p is the plasma length scale, λ_{MW} is the microwave wavelength, R is the observation point distance from the plasma, and δ_d is the electromagnetic skin depth),¹²

$$E_{\text{signal}} \propto \frac{n_e}{\sqrt{(\zeta\omega_p^2 - \omega_{MW}^2)^2 + (v_m\omega_{MW})^2}}, \quad (1)$$

where n_e is the number density of electrons in the scattering volume, $v_m = \sum_{\alpha} v_{m\alpha}$ is the total collision frequency of the electrons summed over collisions with species α , $\omega_p = \sqrt{n_e e^2 / (m_e \epsilon_0)}$ is the plasma frequency, and m_e is the electron mass. The depolarization factor¹³ ζ captures the electric polarization effects due to the geometry of the small REMPI-generated plasma. We can approximate the REMPI-generated plasma as a prolate ellipsoid with semiminor axes given by the beam waist $w_0 \approx 50 \mu\text{m}$ and the semimajor axis given by the Rayleigh range $z_R \approx 2 \text{ mm}$. The ellipsoid eccentricity is $e_{\text{ellipsoid}} = \sqrt{1 - (w_0/z_R)^2} \approx 0.9997$, which results in a depolarization factor $\zeta \approx 2 \times 10^{-3}$ for incident microwave polarization along the semimajor axis. As a result of the small depolarization factor, the higher collisionality regime of experiments of interest ($v_m \gg \omega_{MW}$, where $\omega_{MW} = 2\pi/\lambda_{MW}$ is the microwave angular frequency), and the smaller density of electrons near the ends of the ellipsoid, we can neglect the restoring force that is due to the formation of the charged sheath on the plasma edges and hence obtain a simpler expression for Eq. (1),

$$E_{\text{signal}}(t) \propto \frac{n_e(t)}{v_m(t)}. \quad (2)$$

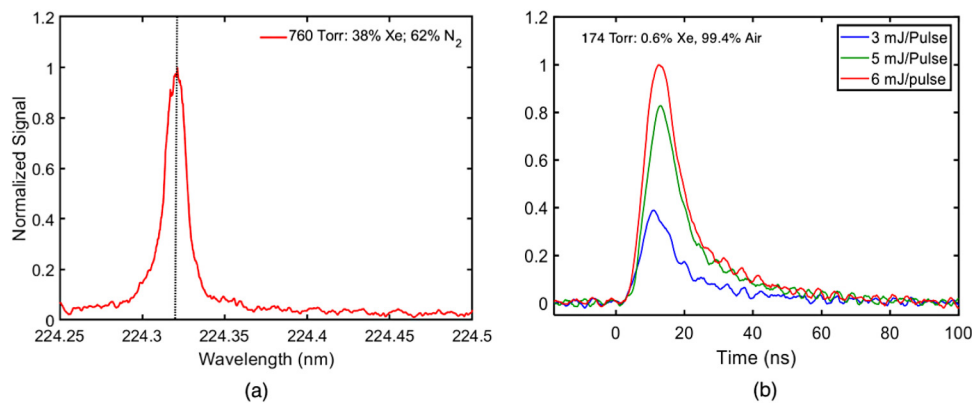


FIG. 3. (a) REMPI spectrum of xenon in a 760 Torr xenon–nitrogen mixture as measured by coherent microwave scattering and scanning the dye laser wavelength output. (b) Microwave scattering waveforms for scattering on REMPI in a 174 Torr xenon–air mixture.

We will use Eq. (2) to model the Radar REMPI signal for a 1 Torr xenon, 173 Torr air mixture given various input laser energies, and compare our models with experiment.

A. REMPI modeling

A laser pulse of 224.32 nm wavelength is focused to ionize xenon via 2 + 1 REMPI ionization (two-photon excitation to the resonance excited state + one-photon ionization from this excited state). In order to model the 2 + 1 REMPI ionization in our kinetic model, we require the two-photon excitation and one-photon ionization cross sections for 224.32 nm photons with $5p^56p'[3/2]_2$ as the resonance excited state (energy level obtained from NIST¹⁴).

We first calculate the two-photon excitation rate. The transition probability rate from the ground state $|g\rangle = 5p^61S_0$ to the resonance excited state $|f\rangle = 5p^56p'[3/2]_2$ is given by

$$W_{fg}^{(2)} = \sigma^{(2)}F^2, \quad (3)$$

where $\sigma^{(2)} = \sigma_0^{(2)}g(\omega_L)$ is the two-photon excitation cross section, $F = I/(\hbar\omega_L)$ is the photon flux (I is the incident laser irradiance and ω_L is the laser angular frequency), $\sigma_0^{(2)}$ is the corresponding normalized cross section, and $g(\omega_L)$ is the line shape function at line-center,

$$g(\omega_L) = \frac{2\sqrt{\ln(2)/\pi}}{\sqrt{2(\Delta\omega_L)^2 + (\Delta\omega_T)^2}}, \quad (4)$$

where $\Delta\omega_L$ is the incident laser bandwidth and $\Delta\omega_T$ is the transition Doppler bandwidth. We do not include pressure broadening here since the mean collision rate of air molecules at 173 Torr is on the order of GHz, which is much less than the laser bandwidth of order 100 GHz mentioned in Sec. II. The normalized two-photon excitation cross section is $\sigma_0^{(2)} \approx 4.9 \times 10^{-42} \text{ m}^4$.¹⁵ Estimating a laser bandwidth in a wavelength of the order of magnitude $\Delta\lambda_L \approx 1 \times 10^{-11} \text{ m}$ from the specifications in Sec. II, we obtain $g(\omega_L) \approx 1.8 \times 10^{-12} \text{ s}$, and hence, the two-photon excitation cross section is $\sigma^{(2)} \approx 8.8 \times 10^{-56} \text{ m}^4 \text{ s}$.

The cross section for the one-photon ionization (photoionization) from the $5p^56p'[3/2]_2$ excited state of xenon is calculated using the quantum-defect approximation,¹⁶

$$\sigma_{pi} = \frac{8 \times 10^{-22}}{(U_I/R_\infty)^{1/2}(\hbar\omega_L/U_I)^3}, \quad (5)$$

where U_I is the ionization potential from the two-photon excited state $\approx 1.70 \times 10^{-19} \text{ J}$ ($=1.06 \text{ eV}$) and R_∞ ($=13.6 \text{ eV}$) is the Rydberg constant. We calculated the photoionization cross section to be $\sigma_{pi} = 2.02 \times 10^{-23} \text{ m}^2$. The corresponding transition probability rate can be written in terms of σ_{pi} ,

$$W_{ioniz-f} = \sigma_{pi}F. \quad (6)$$

We now consider the plasma kinetics in order to model the evolution of the Radar REMPI signal [Eq. (2)] utilizing the REMPI cross sections we obtained.

B. Plasma kinetics

The REMPI-generated plasma is modeled as a nonequilibrium plasma containing the following species: electrons (e), neutral xenon atoms (Xe), ions (Xe^+), two-photon excited state atoms (Xe^*), and dimer ions (Xe_2^+); diatomic oxygen negative/positive ions (O_2^-/O_2^+); and neutral diatomic oxygen (O_2) and nitrogen (N_2) molecules. The electron temperature T_e and N_2 vibrational temperature T_v are allowed to vary in time, while the rest of the species temperatures are constant, with $T_{Xe} = T_{Xe^+} = T_{Xe^*} = T_{Xe_2^+} = T_{O_2^-} = T_{O_2^+} = T_{air} = T_0$ ($\approx 293 \text{ K}$) $\leq T_e$. T_e is allowed to vary due to substantial heating of the electrons due to the interaction with the laser pulse via ionization and Joule heating, while T_v is allowed to vary because of the large cross section of the electron-vibrational energy exchange, which acts as one of the main cooling mechanisms for the electrons in collisions with molecular species when $T_e \geq 0.5 \text{ eV}$. Since the gas is weakly ionized, the amount of thermal energy from the electrons is not sufficient to substantially heat the background atoms and ions; therefore, we can take the rest of the species temperatures to remain constant around room temperature.

The electron temperature initial condition is found from setting: $\frac{3}{2}kT_e(0) = \varepsilon_{ph}$, signifying that the excess energy from the third photon in the 2 + 1 REMPI process [$\varepsilon_{ph} = \hbar\omega_L - U_I \approx 7.16 \times 10^{-19} \text{ J}$ ($=4.47 \text{ eV}$)] is divided among the three degrees of freedom of the newly freed electron. The N_2 vibrational temperature T_v is initially in equilibrium with the rest of the gas temperatures $T_v(0) = T_0$. For the initial densities: $n_{air}(0) = 5.7 \times 10^{24} \text{ m}^{-3}$ (173 Torr) and $n_{Xe}(0) = 3.3 \times 10^{22} \text{ m}^{-3}$ (1 Torr). $n_{O_2} = 0.2095n_{air}$ and $n_{N_2} = 0.7809n_{air}$ are the corresponding fractional densities of O_2 and N_2 in air. The rest of the species are initially absent before the ionizing laser pulse: $n_{Xe^+}(0) = n_{Xe^*}(0) = n_{Xe_2^+}(0) = n_{O_2^-}(0) = n_{O_2^+}(0) = 0$, and the air density is taken to be constant $n_{air}(t) = n_{air}(0)$.

The rate equations for the electrons, xenon ions, two-photon excited state atoms, and dimer ions, and negative and positive O_2 ions are, respectively,

$$\begin{aligned} \frac{dn_e}{dt} = & n_{Xe^*}\sigma_{pi}F + v_{avalanche} + v_{pd} - v_{attach}n_e - \beta_{eff}n_en_{Xe^+} \\ & - \beta_{dis}n_en_{Xe_2^+} - \beta_{dis2}n_en_{O_2^+}, \end{aligned} \quad (7)$$

$$\frac{dn_{Xe^+}}{dt} = n_{Xe^*}\sigma_{pi}F - \beta_{eff}n_en_{Xe^+} - k_{convXe}n_{Xe^+}n_{Xe}^2 - k_{iiO_2^-Xe^+}n_{O_2^-}n_{Xe^+}, \quad (8)$$

$$\frac{dn_{Xe^*}}{dt} = n_{Xe}\sigma^{(2)}F^2 - n_{Xe^*}\sigma_{pi}F - k_enen_{Xe^*} - k_{qN_2}n_{N_2}n_{Xe^*}, \quad (9)$$

$$\frac{dn_{Xe_2^+}}{dt} = k_{convXe}n_{Xe^+}n_{Xe}^2 - \beta_{dis}n_en_{Xe_2^+}, \quad (10)$$

$$\frac{dn_{O_2^-}}{dt} = v_{attach}n_e - v_{pd} - k_{iiO_2^-Xe^+}n_{O_2^-}n_{Xe^+} - k_{iiO_2^-O_2^+}n_{O_2^-}n_{O_2^+}, \quad (11)$$

$$\frac{dn_{O_2^+}}{dt} = v_{avalanche} - k_{iiO_2^-O_2^+}n_{O_2^-}n_{O_2^+} - \beta_{dis2}n_en_{O_2^+}, \quad (12)$$

where β_{eff} is the effective recombination rate between electrons and xenon ions, including three-body collisional-radiative recombination with electrons as the third body and two-body photorecombination,¹⁷

$$\beta_{eff} = 1.7 \times 10^{-20}T_e^{-4.5}n_e + 3.02 \times 10^{-16}T_e^{-0.75} [\text{m}^3/\text{s}], \quad (13)$$

and β_{dis} is the dissociative recombination rate between electrons and xenon dimer ions,¹⁸

$$\beta_{dis} = 2.3 \times 10^{-12}(300/T_e)^{0.6}n_e [\text{m}^3/\text{s}]. \quad (14)$$

Xe_2^+ is produced by the conversion reaction of Xe^+ in triple collisions with two Xe atoms with rate constant $k_{convXe} = 3.6 \times 10^{-43} \text{m}^6/\text{s}$.¹⁷ $\epsilon^* \approx 17.71 \times 10^{-19} \text{J}$ ($=11.07 \text{eV}$) is the energy of the two-photon excited state with respect to the ground level. $k_e = 6 \times 10^{-15} \text{m}^3/\text{s}$ and $k_{qN_2} = 5 \times 10^{-16} \text{m}^3/\text{s}$ are the estimated quenching rate constants of the excited state by electrons and N_2 molecules, respectively.^{19,20} The neutral xenon number density can be found from the other number densities by $n_{Xe}(t) = n_{Xe}(0) - n_{Xe^+}(t) - n_{Xe^*}(t) - 2n_{Xe_2^+}(t)$. v_{attach} is the electron attachment rate to O_2 to create negative O_2 ions (O_2^-), which can be assisted by a third body of either O_2 ,

$$v_{attachO_2} = 1.4 \times 10^{-41} \left(\frac{300}{T_e}\right) \exp\left(-\frac{600}{T_0}\right) \times \exp\left(\frac{700(T_e - T_0)}{T_e T_0}\right) n_{O_2}^2 [\text{s}^{-1}], \quad (15)$$

or N_2 ,

$$v_{attachN_2} = 1.07 \times 10^{-43} \left(\frac{300}{T_e}\right) \exp\left(-\frac{70}{T_0}\right) \times \exp\left(\frac{1500(T_e - T_0)}{T_e T_0}\right) n_{O_2} n_{N_2} [\text{s}^{-1}], \quad (16)$$

where $v_{attach} = v_{attachO_2} + v_{attachN_2}$.²¹ $k_{iiO_2^-Xe^+}$ is the ion-ion recombination rate between Xe^+ and O_2^- , which is approximated

$$v_{ev} = \begin{cases} 3.87 \times 10^{-14} n_{N_2} \exp(-1.5/T_e [\text{eV}]) [\text{s}^{-1}], & T_e [\text{eV}] \leq 1 \text{ eV}, \\ (A + 7.5 \times 10^{-15} (1 - 0.036 T_e [\text{eV}])) n_{N_2} / T_e [\text{eV}] [\text{s}^{-1}], & T_e [\text{eV}] > 1 \text{ eV}, \end{cases} \quad (20)$$

where

$$A = 2.13 \times 10^{-13} (T_e [\text{eV}])^{1/2} (1 - 0.05(T_e [\text{eV}] - 4)) \exp(-7.86/T_e [\text{eV}]).$$

$v_{VT} = (23f_{N_2} + 210f_{O_2})p [\text{atm}] [\text{s}^{-1}]$ is the vibrational-translational relaxation rate via N_2-N_2 and N_2-O_2 collisions.²⁴

as the $O_2^-O_2^+$ recombination rate found in the literature,²¹ i.e., $k_{iiO_2^-Xe^+} \approx k_{iiO_2^-O_2^+} = 2 \times 10^{-13} \text{m}^3/\text{s}$. $v_{pd} = n_{O_2^-} \sigma_{pd} F$ is the photodetachment rate, where the photodetachment cross section $\sigma_{pd} = 8 \times 10^{-22} \text{m}^2$ is extrapolated from Ref. 22. $\beta_{dis2} = 2 \times 10^{-13} (300/T_e) \text{m}^3/\text{s}$ is the dissociative recombination rate between electrons and O_2^+ ions.²¹ $v_{avalanche} = J_L / \epsilon_{ionizO_2}$ is the avalanche ionization rate for O_2^+ , where J_L is defined in the next paragraph and $\epsilon_{ionizO_2} = 12.07 \text{eV}$ is the ionization potential of O_2 . Since the ionization potential of O_2 is lower than that of N_2 ($\epsilon_{ionizO_2} = 12.07 \text{eV} < 15.58 \text{eV} = \epsilon_{ionizN_2}$), there would be less avalanche ionization of N_2 ; therefore, we neglect this contribution. We do not consider avalanche ionization of Xe since the amount of xenon is two orders of magnitude lower than the amount of O_2 , and the avalanche ionization rate is directly proportional to species concentration.¹⁸

We include the electron energy and N_2 vibrational energy equations,

$$\frac{d}{dt} \left(\frac{3}{2} n_e k T_e \right) = J_L + n_{Xe^*} \sigma_{pi} F \epsilon_{ph} + k_e n_e n_{Xe^*} \epsilon^* - \frac{3}{2} n_e k (T_e - T_0) \sum_{\alpha} v_{m\alpha} \delta_{\alpha} - \frac{3}{2} n_e k (T_e - T_v) v_{ev}, \quad (17)$$

$$\frac{d}{dt} \left(\frac{3}{2} n_{N_2} k T_v \right) = \frac{3}{2} n_e k (T_e - T_v) v_{ev} - \frac{3}{2} n_{N_2} k (T_v - T_0) v_{VT}, \quad (18)$$

where J_L represents Joule heating from the interaction between the laser pulse and the electrons,

$$J_L = \frac{e^2 n_e I(t) v_m}{\epsilon_0 c m_e (\omega_L^2 + v_m^2)}. \quad (19)$$

$I(t)$ is the laser pulse intensity as a function of time, approximated as a Gaussian profile $I(t) = I_0 \exp(-(t - t_{peak})^2 / 2\sigma_{pulse}^2)$ where the pulse width $\sigma_{pulse} \approx 4 \text{ns}$, and t_{peak} is chosen to be $\approx 12.5 \text{ns}$ so that the majority of the Gaussian pulse occurs after $t = 0$. I_0 is the peak intensity of the pulse, which for an energy per pulse of $E_{pulse} \approx 5 \text{mJ}$ and beam waist $w_0 \approx 50 \mu\text{m}$, we obtain $I_0 \approx 5 \times 10^{13} \text{W/m}^2$ as the proper normalization so that the total time integral of $I(t)$ equals the total pulse energy divided by the cross-sectional area. (For the other two experimental cases of 3 mJ and 6 mJ, $I_0 \approx 3 \times 10^{13} \text{W/m}^2$ and $6 \times 10^{13} \text{W/m}^2$, respectively.) $\delta_{\alpha} = 2m_e/M_{\alpha}$ is the energy loss fraction for an electron in elastic collision with species α , where M_{α} is the mass of species α , not including electrons. v_{ev} is the electron-vibration excitation rate given by²³

The collision frequencies include electron–neutral collisions with air molecules (O_2 and N_2) and xenon atoms and Coulomb collisions with xenon ions,

$$v_{m_{air}} = v_{eN_{air}}, \quad (21)$$

$$v_{m_{Xe}} = v_{eN_{Xe}} + v_{C_{Xe^+}}, \quad (22)$$

where the electron–neutral collision frequency with air $v_{eN_{air}}$ is obtained by fitting the data from 0 to 5 eV,²⁵

$$v_{eN_{air}} = (-4 \times 10^{-16}(T_e[\text{eV}])^4 + 7 \times 10^{-15}(T_e[\text{eV}])^3 - 4 \times 10^{-14}(T_e[\text{eV}])^2 + 1 \times 10^{-13}T_e[\text{eV}])n_{air}[\text{s}^{-1}] \quad (23)$$

($T_e[\text{eV}]$ indicates T_e in units of electron volts). The electron–neutral collision frequency with xenon $v_{eN_{Xe}}$ is given by²⁶

$$v_{eN_{Xe}} = \begin{cases} 1.34 \times 10^{-12} T_e^{-0.495} n_{Xe}[\text{s}^{-1}], & 2.5 \times 10^2 \text{ K} \leq T_e \leq 10^3 \text{ K}, \\ (2.13 \times 10^{-10} T_e^{-1.23} + 4.52 \times 10^{-26} T_e^{3.2}) n_{Xe}[\text{s}^{-1}], & 10^3 \text{ K} \leq T_e \leq 8 \times 10^3 \text{ K}, \end{cases} \quad (24)$$

and the electron–xenon ion Coulomb collision frequency is given by²⁷

$$v_{C_{m^+}} = 2.91 \times 10^{-6} n_{Xe^+} \ln \Lambda / T_e^{3/2} [\text{s}^{-1}], \quad (25)$$

where $\ln \Lambda$ is the Coulomb logarithm ($\Lambda = 12\pi n_e \lambda_D^3$ for electron–ion collisions) and $\lambda_D = \sqrt{\epsilon_0 k T_e / (n_e e^2)}$ is the Debye length. We integrate the aforementioned differential equations in time using the fourth-order Runge–Kutta method to model the Radar REMPI signal waveform [Eq. (2)] for input laser energies of 3 mJ, 5 mJ, and 6 mJ. The results are compared with experiment in Sec. V.

V. RESULTS AND DISCUSSION

Figure 4 shows the simulation results of the number densities of various key species in the mixture of 1 Torr Xenon and 173 Torr air by 3 mJ laser pulse at the center of the laser beam. It

clearly shows that the neutral xenon is excited to the upper states and ionized by the laser pulse within the duration of the laser pulse. Xe_2^+ is formed by three-body collisions. The neutral xenon at the center position recovers by three-body recombination after the laser pulse passes. Other key species of O_2^+ and O_2^- are formed as well. O_2^+ is formed by avalanche ionization mainly during the laser pulse (which can be understood as the electrons from xenon ionization causing the avalanche ionization of O_2 in air during the laser pulse) and then recombines with electrons after the pulse. O_2^- is formed by electron attachment to O_2 during and after the laser pulse and lasts longer than O_2^+ . Formation of cluster ions O_4^+ is very slow at 174 Torr and thus not included.

The experimental and simulation results are compared for 1 Torr xenon 173 Torr air mixtures with an initial laser pulse energy of 3 mJ, 5 mJ, and 6 mJ, shown in Fig. 5. Each of the cases is shown to be in good agreement, although the simulation peaks are broader. This may be due to extensive heating of the electrons, which should be better treated in a 1D model. The 1D model

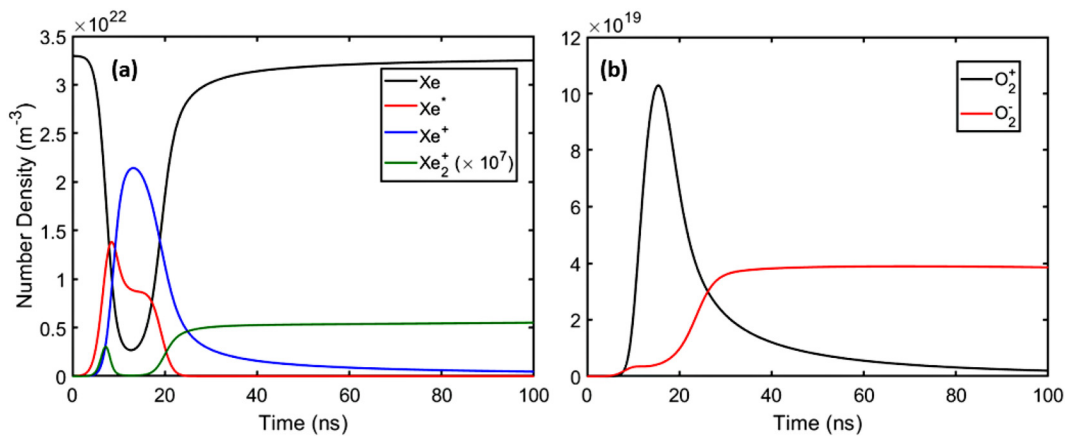


FIG. 4. Number densities of (a) various xenon and (b) molecular oxygen states resulting from the model.

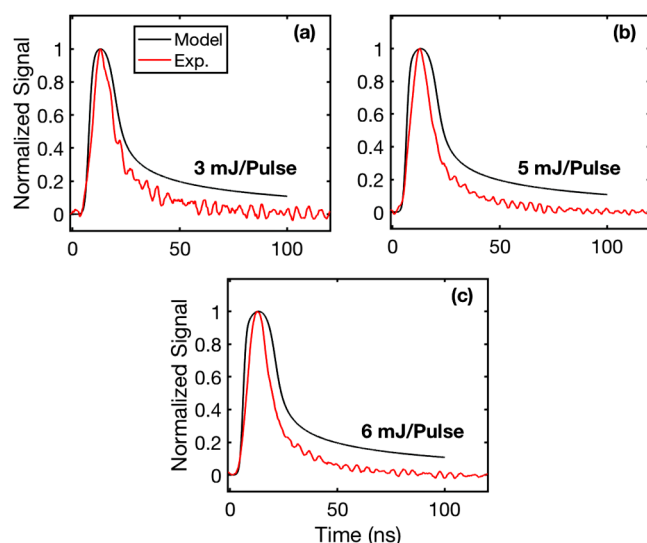


FIG. 5. Comparison of the 0-dimensional kinetic model with experimental results for a 1 Torr xenon 173 Torr air mixture for an incident laser pulse energy of (a) 3 mJ, (b) 5 mJ, and (c) 6 mJ.

would allow expansion of the REMPI plasma, which would result in faster cooling of the electrons via adiabatic cooling. This decrease in the electron temperature would cause a faster decay of the number of electrons [Eq. (13)], which would narrow the simulation peaks in Fig. 5. If we increase the beam area by 50% to simulate a lower intensity pulse (and hence less heating of the electrons), we see better agreement in the width of the peak

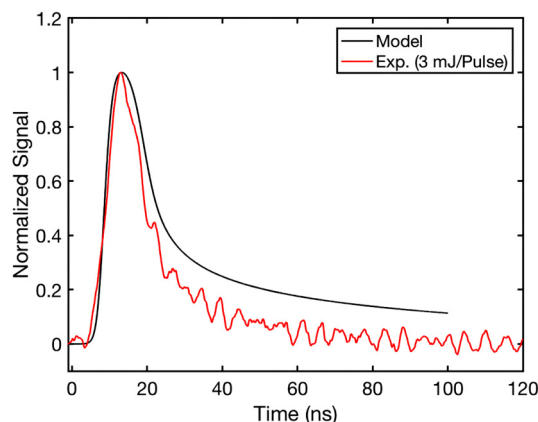


FIG. 6. Comparison of the 0-dimensional kinetic model with experimental results for a 1 Torr xenon 173 Torr air mixture for an incident laser pulse energy of 3 mJ, with reduced intensity to show that our current model may be leading to overheating of the electrons, which could be addressed by incorporating a higher dimensional model and additional reaction rates.

(see Fig. 6). This suggests that heating may play a large role in the broadening of our simulation peaks compared to those of the experimental results, which could be addressed with a higher dimensional model with additional rates included. Nonetheless, there is a broadening of the peak of the experimental results with increasing laser energy, which is captured in the simulation results. We do not see appreciable avalanche ionization in the model—the maximum number density of O_2^+ is two orders of magnitude below the number density of Xe^+ . Appreciable avalanche ionization would require a higher laser intensity or longer pulse duration.

VI. SUMMARY AND CONCLUSIONS

In summary, experimental measurements of xenon REMPI in a 174 Torr xenon–air mixture were made by coherent microwave scattering. Xenon was excited by two photons of 224.3 nm to the 6p state and ionized by the third photon at 224.3 nm. The coherent microwave scattering was used to track the plasma evolution in air. The experimental results were compared with a 0-dimensional model coupled with plasma chemistry of N_2 and O_2 . Since the coherent microwave scattering signal is linearly proportional to the electron density, a comparison of the measured signal and electron density evolution was made. The model qualitatively shows good agreement with the shape of the signal but overestimates the rise time and underestimates the recombination tail seen by microwave scattering. The model also had very little avalanche ionization for the prescribed laser pulse conditions. Finally, it was hypothesized that the current model may be leading to the overheating of electrons and that a higher dimensional model should provide better agreement with the experimental results.

The current results will be useful for REMPI-initiated plasma in air, including using xenon as the seeder for further ionization of N_2 and O_2 . Possibly new diagnostics tools based on REMPI-initiated plasma emissions can be developed to track hypersonic flow dynamics.

ACKNOWLEDGMENTS

The current research at UTK was partially supported by National Science Foundation (NSF). The modeling at Princeton was supported by the Air Force Office of Scientific Research (AFOSR) through an SBIR with MetroLaser, Inc.; the Office of Naval Research (ONR); and the Program in Plasma Science and Technology (PPST) at Princeton University. M.N.S. acknowledges partial support by the Princeton Collaborative Low Temperature Plasma Research Facility under the U.S. Department of Energy, Office of Science, Office of Fusion Energy Sciences.

REFERENCES

1. A. Dogariu and R. B. Miles, *Appl. Opt.* **50**, A68–A73 (2011).
2. Z. Zhang, M. N. Shneider, and R. B. Miles, *Phys. Rev. Lett.* **98**, 265005 (2007).
3. Y. Wu, J. Sawyer, Z. Zhang, and S. F. Adams, *Appl. Opt.* **51**, 6864–6869 (2012).
4. M. Gragston, J. Sawyer, S. F. Adams, Y. Wu, and Z. Zhang, *J. Appl. Phys.* **125**, 203301 (2019).
5. Y. Wu, A. Bottom, Z. Zhang, T. M. Ombrello, and V. R. Katta, *Opt. Express* **19**, 23997–24004 (2011).

- ⁶Z. Zhang, M. N. Shneider, S. H. Zaidi, and R. B. Miles, in *38th Plasmadynamics and Lasers Conference* (AIAA, Miami, FL, 2007), p. 4375.
- ⁷Y. Wu, M. Gragston, Z. Zhang, and J. D. Miller, *Opt. Lett.* **42**, 53–56 (2017).
- ⁸M. Gragston, Y. Wu, Z. Zhang, R. D. Stachler, J. S. Heyne, S. Stouffer, and J. D. Miller, in *55th AIAA Aerospace Sciences Meeting* (AIAA, 2017).
- ⁹M. Uddi, N. Jiang, E. Mintusov, I. V. Adamovich, and W. R. Lempert, *Proc. Combust. Inst.* **32**, 929–936 (2009).
- ¹⁰C. R. Carrigan, Y. Sun, and M. D. Simpson, *J. Environ. Radioact.* **196**, 91–97 (2019).
- ¹¹C. A. Galea, M. N. Shneider, T. Chng, A. Dogariu, and R. B. Miles, in *49th AIAA Plasmadynamics and Lasers Conference* (AIAA, Atlanta, GA, 2018), p. 3435.
- ¹²M. N. Shneider and R. B. Miles, *J. Appl. Phys.* **98**, 033301 (2005).
- ¹³L. D. Landau and E. M. Lifshitz, in *Course of Theoretical Physics Volume 8: Electrodynamics of Continuous Media*, 2nd ed. (Pergamon, Amsterdam, 1984), Chap. 1.
- ¹⁴E. B. Saloman, *J. Phys. Chem. Ref. Data* **33**, 765 (2004).
- ¹⁵M. Uddi, N. Jiang, E. Mintusov, I. V. Adamovich, and W. R. Lempert, *Proc. Combust. Inst.* **32**, 929–936 (2009).
- ¹⁶J. Bokor, J. Zavelovich, and C. K. Rhodes, *Phys. Rev. A* **21**, 1453–1459 (1980).
- ¹⁷Y. P. Raizer, in *Gas Discharge Physics*, 1st ed. (Springer-Verlag, Berlin, 1991), Chap. 4.
- ¹⁸M. N. Shneider and R. B. Miles, *Phys. Plasmas* **19**, 083508 (2012).
- ¹⁹A. G. Zhiglinskii, *Reference Book on Constants of Elementary Processes with Atoms, Ions, Electrons, and Photons*, 1st ed. (Saint Petersburg State University, Saint Petersburg, 1994).
- ²⁰U. V. Ivanov, A. M. Pravilov, L. G. Smirnova, and A. F. Vilesov, *J. Photochem. Photobiol. A: Chem.* **54**, 139–158 (1990).
- ²¹I. A. Kossyi, A. Y. Kostinsky, A. A. Matveyev, and V. P. Silakov, *Plasma Sources Sci. Technol.* **1**, 207 (1992).
- ²²L. C. Lee and G. P. Smith, *J. Chem. Phys.* **70**, 1727 (1979).
- ²³M. N. Shneider, A. Baltuska, and A. M. Zheltikov, *J. Appl. Phys.* **110**, 083112 (2011).
- ²⁴E. M. Bazelyan and Y. P. Raizer, *Spark Discharge*, 1st ed. (CRC Press, New York, 1998), Chap. 2.
- ²⁵S. Slinker and A. W. Ali, NRL Memorandum Report 5614, 1985.
- ²⁶P. Baille, J. Chang, A. Claude, R. M. Hobson, G. L. Ograms, and A. W. Yau, *J. Phys. B: At. Mol. Phys.* **14**, 1485–1495 (1981).
- ²⁷J. D. Huba, *Plasma Physics* (Naval Research Laboratory, Washington, DC, 2013), pp. 1–71.